EPJ manuscript No.
(will be inserted by the editor)

Dynamical Complexity in the C.elegans Neural Network

Chris G. Antonopoulos[1], Athanasios S. Fokas[2], and Tassos C. Bountis[3]

[1] Department of Mathematical Sciences, University of Essex, Wivenhoe Park, CO4 3SQ, United Kingdom
[2] Department of Applied Mathematics and Theoretical Physics, University of Cambridge, Cambridge, CB3 0WA, United Kingdom
[3] Center for Research and Applications of Nonlinear Systems, Department of Mathematics, University of Patras, Patras, GR-26500, Greece

Abstract. We model the neuronal circuit of the *C.elegans* soil worm in terms of a Hindmarsh-Rose system of ordinary differential equations, dividing its circuit into six communities which are determined via the Walktrap and Louvain methods. Using the numerical solution of these equations, we analyze important measures of dynamical complexity, namely synchronicity, the largest Lyapunov exponent, and the Φ_{AR} auto-regressive integrated information theory measure. We show that Φ_{AR} provides a useful measure of the information contained in the *C.elegans* brain dynamic network. Our analysis reveals that the *C.elegans* brain dynamic network generates *more information than the sum of its constituent parts*, and that attains higher levels of integrated information for couplings for which either all its communities are highly synchronized, or there is a mixed state of highly synchronized and desynchronized communities.

1 Introduction

Single-cell organisms manage to survive without possessing neurons. For example, bacteria in a petri-dish respond to a drop of a toxic substance by clamping together. Presumably, neurons appeared in evolution when multicellular organisms were sufficiently complicated that it became "useful" to have a designated system of communication. Organisms with even very simple nervous systems exhibit more complex behaviors than organisms without neurons. For example, the *C.elegans* soil worms, which have 302 neurons, feed alone if food is available and if the environment is quiet; however, if food is scarce and if they detect a threat (such as an unpleasant odour), they feed in groups. Presumably, this behavior is unconscious [1].

The identification of objective criteria for distinguishing conscious from unconscious processes still remains an important open problem. In recent years, an attempt has been made to "mathematise" consciousness [3–9]. Indeed, in his beautiful book "Phi, a Voyage from the Brain to the Soul" [10], the well-known neuroscientist and psychiatrist G. Tononi claims that the only way to understand consciousness is to express it in terms of mathematical equations. Furthermore, Tononi claims that "consciousness is

integrated information theory", and the latter takes indeed the form of a concrete mathematical expression.

In what follows, we focus on the brain dynamic network (BDN) of the *C.elegans* soil worm [11] whose connectome is almost completely mapped [12]: However, we must point out that the Hindmarsh-Rose (HR) type of neuronal dynamics we impose on our BDN (see Section 3 below) may not be an adequate representation of the "real biology" of the *C.elegans*. Thus, our results should be viewed as indicative of the general behavior expected from a biologically realistic neuronal network. Our work primarily focuses on several quantities that describe the dynamical complexity of this brain network, and after computing these quantities, we make comparisons and draw a number of useful conclusions with respect to chaotic behavior, neural synchronization and a measure that quantifies the amount of integrated information generated by this network. More specifically, we employ concepts of nonlinear dynamics and complexity [13–15] and investigate their possible connections with the notion of integrated information theory [4, 7, 9]. In particular, we apply measures of synchronization [17–21] and chaos [22] with integrated information theory [23] to better analyze and understand the numerical solution of a BDN model describing the *C.elegans* brain.

It is well-known that a defining feature of all neural circuits (including the primitive radiata) is their connectivity. Note that the larger the number of neurons, the larger the number of available connectivity profiles, hence the greater the potential for richer behavior. Neuronal network modeling provides a rigorous mathematical way of quantifying this behavior. Indeed, building on the seminal work of Hodgkin and Huxley [24] there now exist several different systems of ordinary differential equations (ODEs) which can be used to model a given neural circuit. The numerical solution of these ODEs exhibits typical features of the behavior of a neuronal circuit, including chaotic behavior characterized by spiking and bursting.

2 Materials and Methods

2.1 C.elegans Data

C.elegans is a 1mm long soil worm with a simple nervous system that consists of 302 neurons and about 7000 synapses [25]. Its nervous system is divided into two distinct and independent components: A large somatic nervous system and a small pharyngeal nervous system. In the present study, we adopt the connectome of the large somatic nervous system found in Ref. [11] consisting of 277 neurons, and use for simplicity the undirected version of the relevant adjacency matrix. We then couple the different neurons via ODEs using the corresponding adjacency matrix obtained from the brain connectivity of the *C.elegans*.

2.2 The Hindmarsh-Rose Neural Model

We model the dynamics of each "neuron" by a single HR neuron system. Namely, following Refs. [19, 26], we endow the nodes (i.e. neurons) of the *C.elegans* BDN with the dynamics characterized by the following system of ODEs [27]:

$$\begin{aligned} \dot{p} &= q - ap^3 + bp^2 - n + I_{\text{ext}}, \\ \dot{q} &= c - dp^2 - q, \\ \dot{n} &= r[s(p - p_0) - n], \end{aligned} \tag{1}$$

where p is the membrane potential, q characterizes the fast ion current (i.e. Na^+ or K^+), and n the slow ion (adaptation) current, for example Ca^{2+}. In this neuron

system, p, q and n are expressed in dimensionless units [27]. The parameters a, b, c, d, which model the function of the fast ion channels, and s, p_0 are given by $a = 1$, $b = 3$, $c = 1$, $d = 5$, $s = 4$ and $p_0 = -8/5$ (see Refs. [19, 26, 27]) and are the same for all neurons. The parameter r, which modulates the slow ion channels of the system, is set to 0.005 for all neurons, and the parameter $I_{\rm ext}$, which is the current that enters the neuron, is set to 3.25 for all neurons. For the above values, each neuron can exhibit chaotic behavior and the solution for $p(t)$ exhibits typical multi-scale chaos characterized by spiking and bursting activity consistent with the membrane potential observed in experiments on single neurons *in vitro* [27]. Thus, chaos not only allows the simulated BDNs to reproduce behaviors empirically observed in experiments with single neurons, but also allows the network to process information generated via an external stimulus [28].

Since the neuron activity of *C.elegans* is not generally expected to be spiking, we carried out the same study at another parameter point ($b = 2.5, I_{ext} = 3.5$) supporting only bursting behavior. In particular, we have considered three characteristic coupling pairs in the parameter space of Fig. 1, one in the yellow region of high synchronization, $(g_n, g_l) = (0.02, 1.7)$, one in the blue region of low synchronization $(g_n, g_l) = (0.1, 0.3)$ and a third at $(g_n, g_l) = (0.23, 1.6)$ in the red region of large dynamical instability. Our results regarding the integrated information measures $\Phi_{\rm AR}$ are very similar to what we have found at the other pair of parameters (with the exception of $\Phi^q_{\rm AR}$ in the red region being one order of magnitude higher). Thus, we feel that our findings are not strongly affected by whether the dynamics is in the spiking or bursting regimes, even though this is an interesting point that requires further investigation.

We couple the HR system to create an undirected BDN of N_n neurons connected simultaneously by linear diffusive coupling and nonlinear coupling synapses [26] as follows:

$$\begin{aligned}
\dot{p}_i &= q_i - a p_i^3 + b p_i^2 - n_i + I_{\rm ext} - g_n (p_i - V_{\rm syn}) \sum_{j=1}^{N_n} \mathbf{B}_{ij} S(p_j) - g_l \sum_{j=1}^{N_n} \mathbf{G}_{ij} H(p_j), \\
\dot{q}_i &= c - d p_i^2 - q_i, \\
\dot{n}_i &= r[s(p_i - p_0) - n_i], \\
\dot{\phi}_i &= \frac{\dot{q}_i p_i - \dot{p}_i q_i}{p_i^2 + q_i^2},\ i = 1, \ldots, N_n,
\end{aligned} \tag{2}$$

where $\dot{\phi}_i$ is the instantaneous angular frequency of the i-th neuron, with ϕ_i being the phase defined by the fast variables (p_i, q_i) of the i-th neuron [29]. The functions H and S are chosen as $H(p_i) = p_i$ and $S(p_j) = [1 + e^{-\lambda(p_j - \theta_{\rm syn})}]^{-1}$ [19, 26]. S is a sigmoidal function that acts as a continuous mechanism for the activation and deactivation of the chemical synapses and, also allows for analytical calculations of the synchronous modes and synchronization manifolds of the coupled system of Eqs. (2) [19]. The remaining parameters are chosen as follows: For the parameters $\theta_{\rm syn}$, λ, and $V_{\rm syn}$, we set $\theta_{\rm syn} = -0.25$, $\lambda = 10$, and $V_{\rm syn} = 2$ is chosen so as to yield an excitatory BDN [19, 26].

The parameters g_n and g_l, which are varied in the parameter spaces of all figures of the paper, denote the strength associated with the nonlinear excitatory and linear diffusive coupling between the corresponding synapses, respectively, and are assigned after the break-down of the brain network into communities, for both community detection methods used in this work (see Subsec. 2.5).

Regarding the physical meaning of these parameters, we note that the authors in Ref. [12] have suggested that there exist chemical and self-consistent gap junction synapse networks in the *C.elegans* brain. In our model, we have used a simplified

version, in which neurons in different communities are coupled chemically (through nonlinear excitatory connections) whereas those in the same community are coupled electrically (through linear diffusive connections). It would be interesting to extend our study to more complex brain networks such as those described in Ref. [12].

For the chosen parameters, we have taken $|p_i| < 2$, and $(p_i - V_{\rm syn})$ always negative for excitatory networks. If two neurons are connected via an excitatory synapse, then if the presynaptic neuron spikes, it induces the postsynaptic neuron to spike. We adopt only excitatory nonlinear synapses in our analysis. $\mathbf{G}_{ij}$ accounts for the way neurons are linearly (diffusively) coupled and is represented by a Laplacian matrix

$$\mathbf{G}_{ij} = \mathbf{K}_{ij} - \mathbf{A}_{ij}, \tag{3}$$

where $\mathbf{A}$ is the binary adjacency matrix of the linear connections and $\mathbf{K}$ is the degree identity matrix based on $\mathbf{A}$; thus $\sum_{j=1}^{N_n} \mathbf{G}_{ij} = 0$. By binary we mean that if there is a connection between two neurons then the entry of the matrix is 1, otherwise it is 0. $\mathbf{B}_{ij}$ is a binary adjacency matrix and describes how the neurons are nonlinearly connected and therefore its diagonal elements are equal to 0, thus $\sum_{j=1}^{N_n} \mathbf{B}_{ij} = k_i$, where k_i is the degree of the i-th neuron, i.e. k_i represents the number of nonlinear links that neuron i receives from all other j neurons in the network. A positive off-diagonal value of both matrices in row i and column j means that neuron i perturbs neuron j with an intensity given by $g_l \mathbf{G}_{ij}$ (linear diffusive coupling) or by $g_n \mathbf{B}_{ij}$ (nonlinear excitatory coupling). Therefore, the binary adjacency matrix $\mathbf{C}$ of the complex networks considered in this work is given by

$$\mathbf{C} = \mathbf{A} + \mathbf{B}. \tag{4}$$

We use as initial conditions for each neuron i the following: $p_i = -1.30784489 + \eta_i^r$, $q_i = -7.32183132 + \eta_i^r$, $n_i = 3.35299859 + \eta_i^r$ and $\phi_i = 0$, where η_i^r is a uniformly distributed random number in $[0, 0.5]$ for all $i = 1, \ldots, N_n$ (see Refs. [19,26] for details). These initial conditions have been chosen so that the dynamics will eventually lead to one of the many possible attractors that coexist in the phase space of the system. It does not make any difference though which attractor is chosen, since for all of them a similar dynamical behavior is observed. Thus, there is less need to consider longer transients.

2.3 Numerical Simulations Details

We have integrated numerically Eqs. (2) using the Euler integration method (first order) with time step $\delta t = 0.01$. We have decided to employ a first order scheme in order to reduce the numerical complexity and CPU time of the required simulations to feasible levels. A preliminary comparison of the trajectories computed for the same parameters (i.e. δt, initial conditions, etc.) via integration methods of order 2, 3 and 4 produced similar results.

We have calculated the largest Lyapunov exponent λ_1 using the well-known method of Ref. [22]. The numerical integration of the HR system of Eqs. (2) was performed for a total time of $t_f = 5000$ units and the computation of the various quantities needed in our analysis, such as the largest Lyapunov exponent λ_1, were computed after a transient time $t_t = 300$ in order to make sure that orbits have converged to an attractor of the dynamics.

2.4 Synchronization Measures in BDNs

It is known that burst synchronization of neural systems can be strongly influenced by many factors, including coupling strengths and types [17], noise [30], and the

existence of clusters in neural networks [31]. Here, we use the order parameter ρ to account for the synchronization level of the neural activity of the *C.elegans* BDN and its communities [18]. This notion, which originates from the theory of measures of dynamical coherence of a population of N_n oscillators of the Kuramoto type [32], can be computed via the expression [18]

$$z(t) = \rho(t)e^{\mathrm{i}\Psi(t)} = \sum_{j=1}^{N_n} e^{\mathrm{i}\phi_j(t)}, \tag{5}$$

where N_n denotes the number of neurons of the BDN and $\phi_j(t)$ is the phase variable of the j-th neuron of the HR system given by the fourth equation in Eq. (2). The modulus $\rho(t)$ of the complex number $z(t)$, which takes values in $[0, 1]$, measures the phase coherence of the population of the N_n neurons, and $\Psi(t)$ measures the average phase of the population of oscillators. In fact, we average $\rho(t)$ over time and compute the order parameter $\rho \equiv \langle \rho(t) \rangle_t$ to determine how ρ evolves. The value $\rho = 1$ implies complete synchronization of the oscillators, whereas $\rho = 0$ means complete desynchronization.

We use Eq. (5), adapted accordingly, for the computation of the synchronization level of the *C.elegans* BDN, and of its communities (for a discussion of communities see Subsec. 2.5). In particular, N_n is the number of neurons of the BDN and j runs through all $N_n = 277$ neurons of that network, whereas in the case of communities, N_n represents the number of neurons of the particular community and j refers to the particular neurons which are members of this community.

2.5 Analysis of Networks and Communities

2.5.1 *C.elegans* Brain Network

We have identified the communities of the *C.elegans* brain network using two different approaches: We first used the Walktrap method [33] employing the igraph software using six steps [26], and then the Louvain method [34] (with resolution 1) employing the NetworkX software [35].

The Walktrap algorithm detects communities using a series of short random walks based on the idea that vertices encountered on any given random walk are more likely to lie within a community. The algorithm initially treats each node as its own community, and then merges them into larger communities, followed by still larger ones, and so on. Essentially, given a graph, this algorithm tries to find densely connected subgraphs (i.e. communities) via random walks. The idea is that short random walks tend to stay in the same community. Using the above procedure we have been able to identify 6 communities in the *C.elegans* brain network.

The Louvain algorithm involves two phases: In the first phase, it looks for "small" communities by optimizing modularity locally, and in the second phase the algorithm aggregates nodes of the same community and builds a new network whose nodes are the communities. These steps are repeated iteratively until a maximum of modularity is achieved. By focusing on ad-hoc networks with known community structure, it has been shown that the Louvain method is very accurate. Moreover, due to its hierarchical form which is reminiscent of renormalization strategies, this method allows one to look for communities at different resolutions. The output therefore yields several partitions: The partition found after the first step typically consists of many communities of small sizes; at subsequent steps, larger and larger communities are found due to the aggregation mechanism, and this process naturally leads to a hierarchical decomposition of the network. This algorithm is obviously an approximate method and nothing ensures that the global maximum of modularity is attained.

However, several tests have confirmed that the Louvain algorithm is quite accurate and often provides a decomposition into communities with a modularity close to the optimal. The Louvain algorithm outperforms other methods in terms of computation time, and this allows one to analyze networks of unprecedented size [34]. Following this methodology we were able to identify again 6 communities in the *C.elegans* brain network. However, the communities identified by the Walktrap and Louvain methods are not identical, neither in size nor in their members. This was realized by comparing directly the community structures identified by these methods.

2.6 Integrated Information Theory Measures

In Ref. [23] the authors present some practical methods for measuring integrated information [4] from time-series data. Based on recently introduced measures of integrated information (see for example Refs. [3, 6, 9]), they analyze quantities that measure the extent to which a system generates more information than the sum of its constituent parts as it transitions between different states. The authors in Ref. [23] propose two new such measures, Φ_{E} (empirical) and Φ_{AR} (auto-regressive), that overcome limitations faced by older versions of analogous quantities, and can be computed using time-series data derived from measurements of realistic or model systems. Thus, these measures offer promising approaches for revealing relations between integrated information, consciousness, and other neurocognitive quantities in real and model systems.

The auto-regressive measure Φ (Φ_{AR}) is well-suited for cases where the time-series is non-Gaussian distributed but nevertheless stationary and stochastic. By construction, when applied to Gaussian-distributed, stationary data, it is equivalent to the well-known empirical version of Φ for integrated information, Φ_{E}. However, these measures already differ when applied to non-Gaussian, stationary data. Indeed, Φ_{AR} provides a useful measure of integrated information based on relations between conditional entropy, partial covariance and linear regression prediction error.

Next, we briefly describe the derivation of Φ_{AR} following Ref. [23]: We start from two multivariate random variables $X = (X^1, \ldots, X^n)^T$ and $Y = (Y^1, \ldots, Y^m)^T$, where ^{T} denotes the transpose of a matrix or a vector. Their linear regression is then given by

$$X = a + A \cdot Y + E, \tag{6}$$

where A is the regression matrix, a is a vector of constants, and E the prediction error. E is a random vector uncorrelated with Y. Given that the distributions of X and Y are defined by

$$A = \sum(X, Y) \sum(Y)^{-1}, \tag{7}$$

$$a = \bar{x} - A \cdot \bar{y}, \tag{8}$$

it follows that the linear regression is unique. In this framework, $(Y)^{-1}$ denotes the inverse of the covariance matrix of Y, $\sum(X)$ denotes the $n \times n$ matrix of covariances, $\sum(X, Y)$ the $n \times m$ matrix of cross-covariances, and $\bar{x}$, $\bar{y}$ are the means of the random variables X and Y respectively. E has zero mean and its covariance is the partial covariance of X given Y,

$$\sum(E) = \sum(X|Y) = \sum(X) - \sum(X, Y) \sum(Y)^{-1} \sum(X, Y)^T. \tag{9}$$

Provided that $\sum(Y)$ is an invertible covariance matrix, Eq. (9) holds for any random variables X and Y, whether they are Gaussian or not.

If it happens that X and Y are Gaussian distributed random multivariate variables, then the conditional entropy of X given that $Y = y,\ y \in \mathbb{R}^m$ satisfies the equation

$$H(X|Y=y) = \frac{1}{2}\log\Big(\det\Big(\sum(E)\Big)\Big) + \frac{1}{2}n\log(2\pi e),\ \forall y \in \mathbb{R}^m, \tag{10}$$

where det() denotes the determinant of the matrix. This is a relation between the conditional entropy and linear regression prediction error valid for Gaussian systems. Under these assumptions, the effective information ϕ can be written as

$$\phi\Big[X;\tau,\{M^1,M^2\}\Big] = \frac{1}{2}\log\bigg(\frac{\det(\sum(X))}{\det(\sum(E^X))}\bigg) - \frac{1}{2}\sum_{k=1}^{2}\log\bigg(\frac{\det(\sum(M^k))}{\det(\sum(E^{M^k}))}\bigg), \tag{11}$$

where $\{M^1, M^2\}$ is the bipartition of X, $E^{M^k},\ k = 1, 2$, and E^X are the prediction errors in the linear regressions

$$M^k_{t-\tau} = A^{M^k} \cdot M^k_t + E^{M^k}_t, \tag{12}$$

$$X_{t-\tau} = A^X \cdot X_t + E^X_t. \tag{13}$$

Here, the notation $X_{t-\tau}$ denotes the τ steps past state (i.e. time lag) from the current state X_t.

If the system under consideration is not Gaussian distributed, then Eq. (11) does not hold. However, the right hand side of Eq. (11) is a quantity that is well defined and can be measured empirically. This quantity is actually the basis of the alternative measure Φ_{AR}, i.e. the auto-regressive measure Φ for integrated information proposed in Ref. [23].

Summarizing, we assume that X is a stationary, not necessarily Gaussian, multivariate random variable, and let $\phi_{\mathrm{AR}}\Big[X;\tau,\{M^1,M^2\}\Big]$ represent the right hand side of Eq. (11). Then, Φ_{AR} is simply ϕ_{AR} for the bipartition $\mathcal{B} = \{M^1, M^2\}$ of X that minimizes ϕ_{AR} divided by the normalization factor

$$L(\mathcal{B}) = \frac{1}{2}\log\bigg(\min_k\Big\{(2\pi e)^{|M^k|}\det\Big(\sum\big(M^k\big)\Big)\Big\}\bigg). \tag{14}$$

Under these considerations, $\Phi_{\mathrm{AR}}\big[X;\tau\big]$ is defined by

$$\Phi_{\mathrm{AR}}\big[X;\tau\big] = \phi_{\mathrm{AR}}\big[X;\tau,\mathcal{B}^{\min}(\tau)\big], \tag{15}$$

where

$$\mathcal{B}^{\min}(\tau) = \arg_{\mathcal{B}}\min\left\{\frac{\phi_{\mathrm{AR}}[X;\tau,\mathcal{B}]}{L(\mathcal{B})}\right\}. \tag{16}$$

The function Φ_{AR}, defined by Eq. (15), is formulated in terms of the linear regression prediction error, which essentially compares the whole system to the sum of its parts in terms of the log-ratio of the variance of the past state to the variance of the prediction errors of the linear regression of the past on the present. It can be understood as a measure of the extent to which the present global state of a system is predicted by the past global state, as compared to predictions based on the most informative decomposition of the system into its component parts. In other words, it is a measure that quantifies the extent to which a system generates more information than the sum of its constituent parts.

In closing, it is important to note that in this work we have computed Φ using a *macroscopic* partition of the associated network, as explained in the Results section. For the human brain it is an unproven hypothesis that macro-level Φ results correlate with micro-level Φ values. The interpretation of our results for the *C.elegans* brain, therefore, with respect to integrated information, is based on a similar hypothesis.

A final question, which has not been addressed in the present study, concerns the effect of directionality of information flow in the BDN we have used to analyze the *C.elegans* brain. Currently, we are investigating various directional networks aiming to explore how their dynamics differs from the undirected case and results will appear in a future publication.

3 Results

Our analysis is based on the numerical solution of the ODEs of Eq. (2). Using the Walktrap method, we have divided the *C.elegans* BDN into 6 communities (the Louvain method also produced 6 communities), and have computed the synchronization measure ρ (see Eq. (5)), as well as the synchronization measures $\{\rho_{c_i}\}_1^6$ for each of the 6 communities using both methods. These parameters are plotted in panel (a) (for ρ) and panels (c)-(h) (for ρ_{c_1}-ρ_{c_6}) of Fig. 1 as functions of the nonlinear coupling strength g_n and the linear coupling strength g_l. The former characterizes the strength of the links between the different communities, whereas the latter the strength of the links within each community. These graphs show that for low nonlinear couplings and moderate to higher linear couplings, all communities, as well as the full network become highly synchronized with $\rho > 0.9$ (depicted by the yellow and orange area in the parameter space). This corresponds to the case where the internal synapses within each community are stronger with respect to the synapses that link the different communities. However, this synchronization pattern starts to change as the nonlinear coupling increases to higher values. Interestingly, synchronization patterns start to emerge after $g_n > 0.15$ and for large enough linear couplings: In this regime, the third and sixth communities become synchronized, whereas the other communities remain in a highly desynchronized state. This situation is reminiscent of the so-called "chimera states" that have been recently observed in simple network models of coupled HR oscillators, where synchronized and asynchronous populations are found to coexist [36, 37].

The largest Lyapunov exponent λ_1 is depicted in Fig. 1b). This graph shows that λ_1 is rather large (red region) in the region of the parameter space where the synchronization levels remain quite low. Since higher values of $\lambda_1 (> 0)$ are associated with a higher degree of chaos, this implies an "inverse" relation between synchronization levels and the level of dynamical instability (i.e. chaos) of neural activity. Of course, depending on the coupling strengths, there are also regions where both quantities are low.

We have computed the auto-regressive Φ_{AR} for both the membrane potential $p(t)$ and fast ion current $q(t)$. Indeed, for each pair of values in the plane of nonlinear and linear coupling parameters, the numerical simulation produces a recorded time-series $X^p(t) = \{p_1(t), \ldots, p_{277}(t)\}$ and $X^q(t) = \{q_1(t), \ldots, q_{277}(t)\}$ of the neural activity of all 277 neurons (for an explanation why we used 277 out of 302 neurons see Subsec. 2.1). The *C.elegans* brain network was divided into 6 unequally distributed communities. Thus, it is more convenient for the estimation of Φ^p_{AR} and Φ^q_{AR}, to compute for each community c_i, $i = 1, \ldots, 6$, the following averaged time-series

$$X^p_{c_i}(t) = \frac{1}{|c_i|} \sum_{j \in c_i} X^p_j(t), \tag{17}$$

and

$$X^q_{c_i}(t) = \frac{1}{|c_i|} \sum_{j \in c_i} X^q_j(t), \tag{18}$$

where $|c_i|$ is the number of neurons in community i.

The next step is to prepare the community-averaged time-series in such a way as to be able to calculate $\Phi^p_{\rm AR}$ and $\Phi^q_{\rm AR}$, based on the averaged $X^p_{c_i}$ and $X^q_{c_i}$ versions of the data. Before doing so though, we have performed a preliminary study and have checked that the neural dynamics of the individual neurons of single communities are similar throughout their time-evolution, and that this is valid for all communities, both for the Walktrap and Louvain methods. This allows us to transform $X^p_{c_i}$ and $X^q_{c_i}$ into stationary time-series by performing initially a detrending procedure (subtracting from the time-series their mean), reducing differences in their variance by computing the logarithm with base 10 of $X^p_{c_i}$ and $X^q_{c_i}$, and removing the parts of the trajectories that correspond to quiescent periods (i.e. absence of neural activity such as stereotypical spiking behavior). In this way, we obtain the stationary versions $\bar{X}^p_{c_i}$ and $\bar{X}^q_{c_i}$, which can be seen as multivariate (six variates for each $\bar{X}_{c_i}$) analogues of stochastic-like random stationary processes. These quantities are then used for the estimation of $\Phi^p_{\rm AR}$ and $\Phi^q_{\rm AR}$.

For the estimation of these two quantities we use the Matlab code "ARphidata.m" for stationary data provided in the Supporting Information of Ref. [23]. We thus present the results of these computations for $\tau = 1$ (associated with the Walktrap community detection method) in panels i), j) of Fig. 1. Panel i) is the parameter space for the quantity $\Phi^p_{\rm AR}$ and panel j) for the quantity $\Phi^q_{\rm AR}$. In the context of the integrated information theory of consciousness [3–5, 7], $\Phi_{\rm AR} \geq 0$, being zero when a system generates the same amount of information with the sum of its parts as it transitions between states. If one is to attribute a physical meaning to $\Phi^p_{\rm AR}$ and $\Phi^q_{\rm AR}$, one would say that the higher their values, the higher the level of consciousness. In this sense, we cannot say that a certain value of Φ is small, unless it is compared with other Φ values in the same figure. For this reason, we do not normalize $\Phi^p_{\rm AR}$ and $\Phi^q_{\rm AR}$. We observe that $\Phi^p_{\rm AR}$ reaches high values in the range of low nonlinear and relatively moderate to high linear couplings; these are precisely the values where the synchronization levels of all communities (panels c) to h)) and the whole BDN (panel a)) of the *C.elegans* are also quite high. On the other hand, $\Phi^q_{\rm AR}$ attains high values in the range of high nonlinear and relatively low to high linear couplings; this is the region of parameter space where the synchronization level of the sixth (see panel h)) and possibly the third community (see panel e)) are very high, despite the asynchronous behavior of the rest of the communities.

A similar study for $\tau = 1$ presented in Fig. 2 for the six communities detected by the Louvain method reveals analogous results with those for the Walktrap method shown in Fig. 1. In these two figures, there are, however, some striking differences with regard to the global synchronization ρ and integrated information theory measure $\Phi^p_{\rm AR}$. Indeed, a comparison between Figs. 1a) and 2a) shows that the whole BDN of the *C.elegans* becomes highly synchronized (Fig. 2a)) for $g_n > 0.25$, which is in contrast to what is depicted in Fig. 1a) for the same range of nonlinear couplings. The reason is that the number of nonlinear connections for the Louvain method is larger (742 undirected links) than those of the Walktrap method (586 undirected links). Additionally, the integrated information theory measures $\Phi^p_{\rm AR}$ in Figs. 1i) and 2i) attain their highest values (about 0.3 and 0.4 respectively) for different coupling ranges: Notably, $\Phi^p_{\rm AR}$ is maximal in Fig. 2i) for g_l values in $(1.6, 2)$ and small nonlinear coupling g_n, whereas in Fig. 1i), it is maximal for pairs of couplings for which $g_l > 0.8$

and g_n quite small. On the other hand, when the linear coupling is moderate and the nonlinear coupling large enough (i.e. $g_n \approx 0.28$), Φ^q_{AR} in Figs. 1j) and 2j) attains its highest value (of about 0.09 in both cases). It is well-known that, in the context of the integrated information theory of consciousness, a good practise is to adopt the τ value that maximizes Φ_{AR}. Here, in order to study the effect of different time delays in Φ_{AR}, we have also computed similar parameter spaces for both integrated information theory measures and community detection methods using $\tau = 2, 3, 4$ and 5. Interestingly, we find that the new parameter spaces about both Φ measures for $\tau = 2, 3, 4$ and 5 are qualitatively similar to those for $\tau = 1$ in Figs. 1 and 2, and thus there is no need for choosing those that maximize Φ_{AR}. This similarity for different τ may be due to slow decay of correlations and hence absence of small τ values at which memory effects are minimal.

In conclusion, both measures attain higher levels for couplings for which either all communities are strongly synchronized, or there is a mixed state of highly synchronized and desynchronized communities. Both cases are found to be characterized by low chaotic behavior, as depicted by the maximal Lyapunov exponent.

4 Discussion

In this work we have attempted to quantify and compare certain important measures of dynamical complexity: (i) A measure of synchronicity, which is suggestive of integration between sub-domains as the system exhibits coherent behavior as a whole (see Ref. [38] in which it is shown that when a simple flickering stimulus is consciously perceived there is a marked increase in long-range coherence at the stimulus frequency), (ii) the largest Lyapunov exponent, which provides a measure of chaos (or dynamical instability) and, (iii) Φ^p_{AR} and Φ^q_{AR}, which are the auto-regressive information measures associated with the membrane potential p and fast ion current q, respectively. The latter ones can be understood as measures of the extent to which the present global state of the system reflects the past global state, compared with predictions based on the most informative decomposition of the system into its components.

As argued in Ref. [23], Φ_{AR} possibly reflects levels of consciousness generated by neural systems. It appears that the notion of Φ_{AR} provides a useful tool for quantifying the integrated information contained in a given neural system. Thus, in the context of the integrated information theory of consciousness, if one is to attribute a physical meaning to Φ_{AR}, one would say that the higher its value, the higher the level of consciousness.

Combining the results of Figs. 1 and 2, and based on the above interpretation, our analysis suggests that, for particular coupling strengths, the *C.elegans* BDN is able to generate more information than the sum of its constituent parts. Specifically, we find that the *C.elegans* BDN attains higher levels of integrated information for couplings for which either all its communities are highly synchronized, or there is a mixed state of highly synchronized and desynchronized communities, a situation that corresponds to low chaotic neural behavior. We find that in the case of the *C.elegans* brain network there exist substantial differences between the behaviors of the Φ^p_{AR} and Φ^q_{AR} measures.

A complementary approach has been given in Ref. [26] where various statistical quantities associated with the same *C.elegans* brain network, such as the global clustering coefficient, the average of local clustering coefficients, the mean shortest path, the degree probability distribution function of the network and the small-worldness measure have been computed. Even though small-worldness captures important aspects of complex networks at the local and global scale, it does not provide information

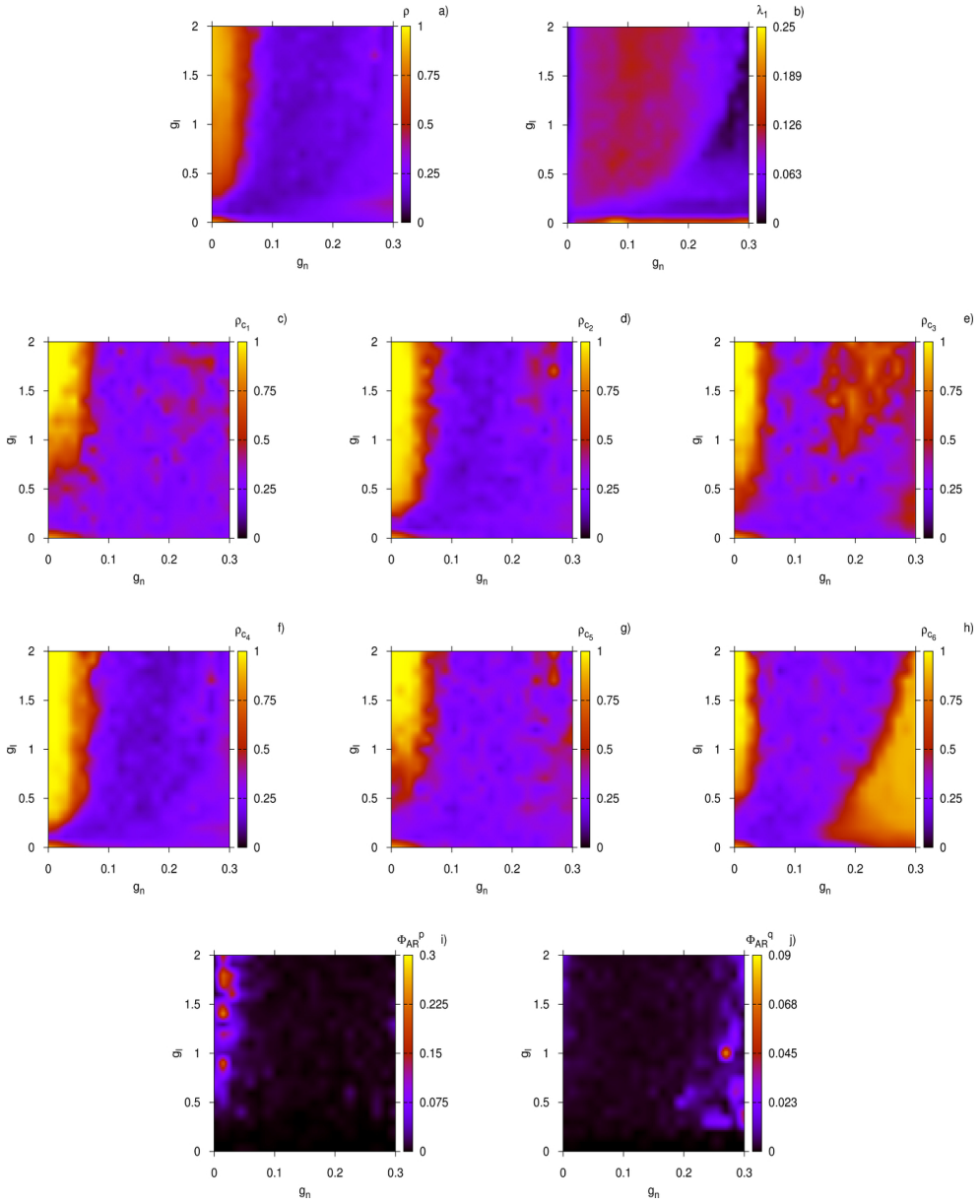

Fig. 1. High synchronization and low dynamical neural instability imply high integrated information theory measure for the *C.elegans* communities detected by the Walktrap method. Panel a) is the parameter space of the synchronization measure ρ for the whole BDN and panel b) is a similar parameter space for the largest Lyapunov exponent λ_1 of the neural dynamics. Panels c) to h) are similar to panel a) for the synchronization measures ρ_{c_1}-ρ_{c_6} of the six communities, respectively. Panels i) and j) show the parameter spaces of the integrated information theory measures Φ^p_{AR} and Φ^q_{AR}, respectively. In all panels, g_n is the nonlinear coupling, g_l the linear coupling, and $\tau = 1$.

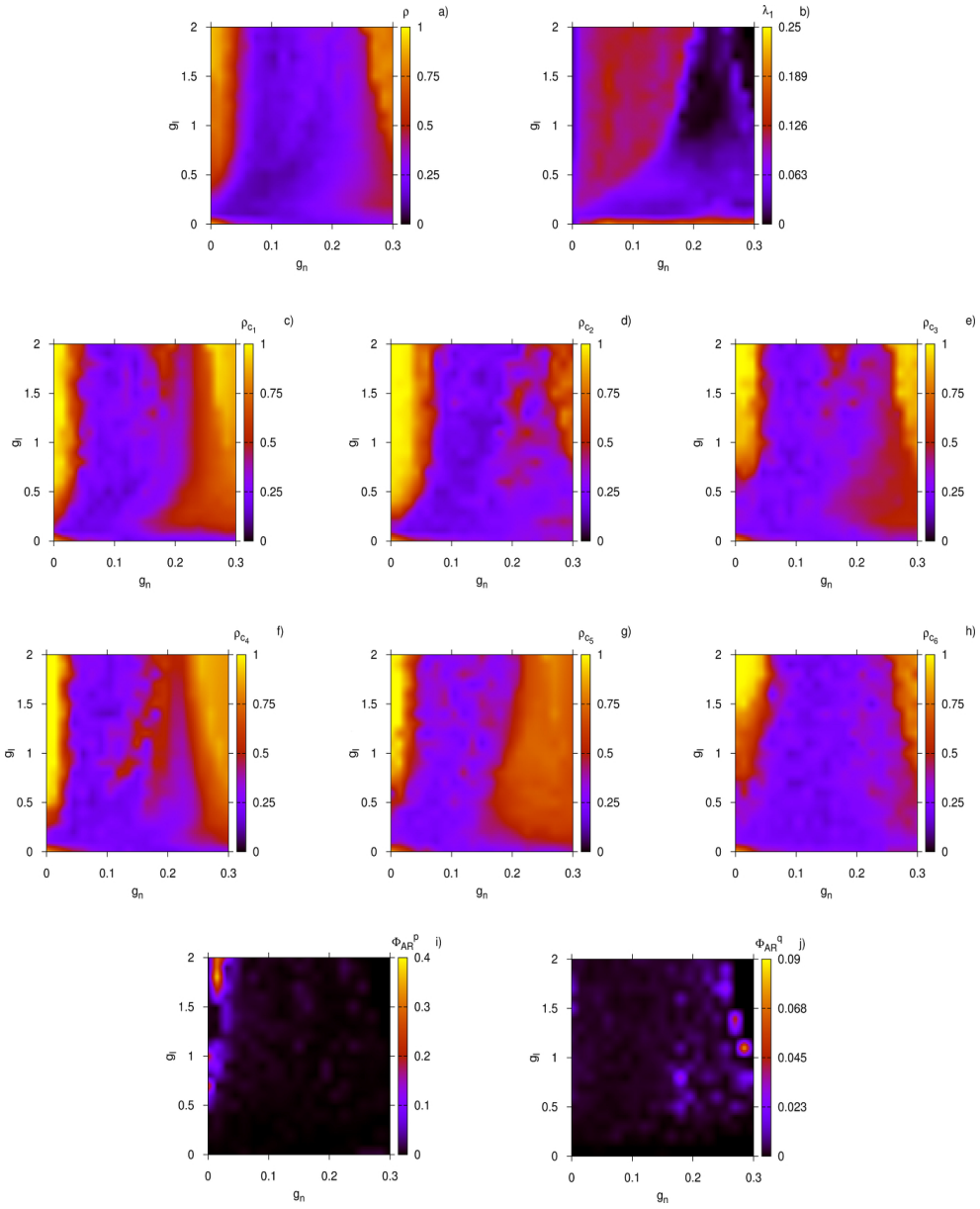

Fig. 2. High synchronization and low dynamical neural instability imply high integrated information theory measure for the *C.elegans* communities detected by the Louvain method. Panel a) is the parameter space of the synchronization measure ρ for the whole BDN and panel b) is a similar parameter space for the largest Lyapunov exponent λ_1 of the neural dynamics. Panels c) to h) are similar to panel a) for the synchronization measures ρ_{c_1}-ρ_{c_6} of the six communities, respectively. Panels i) and j) show the parameter spaces of the integrated information theory measures Φ^p_{AR} and Φ^q_{AR}, respectively. In all panels, g_n is the nonlinear coupling, g_l the linear coupling, and $\tau = 1$.

about the intermediate scale. This can be better described by the modularity, or community structure of the network.

It is also important to note that the authors in Ref. [12] have gathered and combined material from many different sources and studies, and report on the whole set of self-consistent gap junction and chemical synapses of the *C.elegans* brain. They identify neurons that may play a central role in information processing, and network motifs that could serve as functional modules of the brain network. This is in the same spirit with the notion of communities used in the present study, but involves a more complicated distribution of chemical and electrical synapses than we have assumed here. In a future publication, we plan to extend our analysis to investigate dynamical complexity in more "realistic" neural networks, such as those reported in Ref. [12].

It is also interesting to ask to what extent the results of the present study can be attributed to the particular *C.elegans* network used here. As a first step in this direction, we applied the HR dynamics to an Erdős-Rényi random network and found that they are quite different: As shown in Fig. 3, the values of Φ_{AR} differ from what is depicted in Figs. 1 and 2. We also found that the number of communities is also different (9 instead of 6, applying the same community detection methods) as well as the location and extent of regions of synchronization (not shown in Fig. 3).

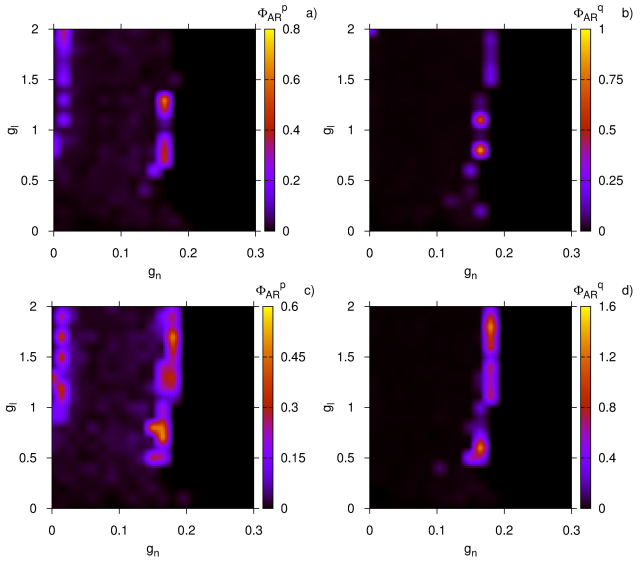

Fig. 3. Results for the integrated information theory measures Φ^p_{AR}, Φ^q_{AR} and time delay $\tau = 5$, for the communities of the Erdős-Rényi random network, detected by the Walktrap and Louvain methods. Panel a) is the parameter space for the integrated information theory measure Φ^p_{AR} and panel b) for Φ^q_{AR}, based on the communities detected by the Walktrap method. Panels c) and d) are similar to a) and b) for the integrated information theory measures Φ^p_{AR} and Φ^q_{AR} respectively, for the communities of the same Erdős-Rényi random network, detected by the Louvain method. In all panels, g_n is the nonlinear and g_l the linear coupling.

Finally, inspired by the findings in Ref. [12] regarding the directionality of electrical and chemical connections in the *C.elegans* brain network, we have made a preliminary study computing the Φ^p_{AR} and Φ^q_{AR} measures for three characteristic coupling pairs in the parameter space of Fig. 1 c)-h). More specifically, since the directionality of gap

junctions (electrical) for the *C.elegans* has not been established, we have assumed that the network of the electrical connections is undirected and hence can be represented by a symmetric matrix $\mathbf{G}$. On the other hand, the chemical connections are thought to be directed [12]. Thus, to investigate the effect of directionality, we have solved Eqs. (2) modifying the symmetric matrix $\mathbf{B}$ of the chemical interactions so as to have 30% and 50% of its $\mathbf{B}_{ij}$ elements equal to 0, while the corresponding $\mathbf{B}_{ji}$ are equal to 1. The results are as follows: At a parameter point (g_n, g_l) in the blue (desynchronized) region the Φ_{AR} values are not significantly changed, while at a point in the yellow (synchronized) region both Φ^p_{AR} and Φ^q_{AR} *increase* indicating greater complexity as uni-directionality increases. On the other hand, for a point on the red boundary between the two regions, while Φ^q_{AR} increases, Φ^p_{AR} *decreases* as the percentage of uni-directionality grows. These results suggest that directionality affects differently the integration information in synchronized and desynchronized domains and hence its implications regarding the level of complexity in these domains needs to be investigated in detail in a future publication.

5 Acknowledgments

We are particularly indebted to the referees for their detailed remarks, critical questions and useful comments which have led to a much improved manuscript. A. S. F. acknowledges support from EPSRC. We would like to thank Dr N. Kouvaris for many fruitful discussions and for providing us the communities and adjacency matrices based on the Louvain community detection method. C. G. A., A. S. F. and T. B. acknowledge that this research has been co-financed by the European Union (European Social Fund - ESF) and Greek national funds through the Operational Program "Education and Lifelong Learning" of the National Strategic Reference Framework (NSRF) - Research Funding Program: THALES - Investing in knowledge society through the European Social Fund. Finally, C. G. A. also acknowledges support by the "EPSRC EP/I032606/1" grant as part of this work was performed during his post in the University of Aberdeen.

References

1. Damasio A. Self Comes to Mind: Constructing the Conscious Brain. Vintage; 2012.
2. Dehaene S, Changeux JP. Experimental and Theoretical Approaches to Conscious Processing. Neuron. 2011;70(2):200–227.
3. Tononi G, Sporns O. Measuring information integration. BMC Neurosci. 2003;p. 31.
4. Tononi G. An information integration theory of consciousness. BMC Neurosci. 2004;5:42.
5. Tononi G. Consciousness, information integration, and the brain. Prog Brain Res. 2005;150:109–126.
6. Balduzzi D, Tononi G. Integrated information in discrete dynamical systems: Motivation and theoretical framework. PLOS Comput Biol. 2008;4(6):e1000091.
7. Tononi G. Consciousness as integrated information: A provisional manifesto. Biol Bull. 2008;215(3):216–242.
8. Balduzzi D, Tononi G. Qualia: The geometry of integrated information. PLOS Comput Biol. 2009;5(8):e1000462.
9. Oizumi M, Albantakis L, Tononi G. From the phenomenology to the mechanisms of consciousness: Integrated information theory 3.0. PLOS Comput Biol. 2014 05;10(5):e1003588.
10. Tononi G. Phi: A voyage from the brain to the soul. Pantheon Books; 2012.
11. ; 2010-2011. [Online; accessed 27-February-2014]. Connectome File Format - Datasets (Version 2.0). Available: http://cmtk.org/viewer/datasets/.

12. Varshney LR, Chen BL, Paniagua E, Hall DH, Chklovskii DB. Structural properties of the "Caenorhabditis elegans" neuronal network. PLOS Comput Biol. 2011;7(2):e1001066.
13. Bar-yam Y. Dynamics of Complex Systems (Studies in Nonlinearity). Westview Press; 2003.
14. Nicolis G, Nicolis C. Foundations of Complex Systems. World Scientific, Singapore; 2007.
15. Fuchs A. Nonlinear Dynamics in Complex Systems. Springer-Verlag Berlin Heidelberg; 2013.
16. Tononi G, Edelman GM. Consciousness and complexity. Science. 1998;p. 1846–1851.
17. Belykh I, Lange E, Hasler M. Synchronization of bursting neurons: What matters in the network topology. Phys Rev Lett. 2005;94:188101.
18. Gómez-Gardeñes J, Zamora-López G, Moreno Y, Arenas A. From modular to centralized organization of synchronization in functional areas of the cat cerebral cortex. PLoS ONE. 2010;5:e12313.
19. Baptista MS, Kakmeni FM, Grebogi C. Combined effect of chemical and electrical synapses in Hindmarsh-Rose neural networks on synchronization and the rate of information. Phys Rev E. 2010;82:036203.
20. Arenas A, Guilera AD, Kurths J, Moreno Y, Zhou C. Synchronization in complex networks. Physics Reports. 2008;469(3):93–153.
21. Benedek M, Bergner S, Könen T, Fink A, Neubauer AC. EEG alpha synchronization is related to top-down processing in convergent and divergent thinking. Neuropsychologia. 2011;49(12):3505–3511.
22. Benettin G, Galgani L, Giorgilli A, Strelcyn JM. Lyapunov characteristic exponents for smooth dynamical systems and for Hamiltonian systems: A method for computing all of them. Part 1: Theory and Lyapunov characteristic exponents for smooth dynamical systems and for Hamiltonian systems: A method for computing all of them. Part 2: Numerical application. Meccanica. 1980;15:9–20, 21–30.
23. Barrett AD, Seth AK. Practical Measures of Integrated Information for Time-Series Data. PLOS Comput Biol. 2011;7:e1001052.
24. Hodgkin AL, Huxley AF. A quantitative description of membrane current and its application to conduction and excitation in nerve. The Journal of physiology. 1952;117:500–544.
25. Gally C, Bessereau JL. C. elegans: Des neurones et des gènes. Med Sci (Paris). 2003;19:725–734.
26. Antonopoulos CG, Srivastava S, Pinto SEdS, Baptista MS. Do Brain Networks Evolve by Maximizing their Information Flow Capacity? PLOS Comput Biol. 2015;11(8):e1004372.
27. Hindmarsh JL, Rose RM. A model of neuronal bursting using three coupled first order differential equations. Proc R Soc London. 1984;Ser. B 221:87–102.
28. Baptista MS, Kurths J. Transmission of information in active networks. Phys Rev E. 2008;77:026205.
29. Pereira T, Baptista MS, Kurths J. Detecting phase synchronization by localized maps: Application to neural networks. Europhysics Letters. 2007;77:40006.
30. Burić N, Todorović K, Vasović N. Influence of noise on dynamics of coupled bursters. Phys Rev E. 2007;75:067204.
31. Prado TdL, Lopes SR, Batista CAS, Kurths J, Viana RL. Synchronization of bursting Hodgkin-Huxley-type neurons in clustered networks. Phys Rev E. 2014;90:032818.
32. Kuramoto Y, Battogtokh D. Coexistence of coherence and incoherence in nonlocally coupled phase oscillators. Nonlinear Phenomena in Complex Systems. 2002;5(4):380–385.
33. Pons P, Latapy M. Computing communities in large networks using random walks. Lecture Notes in Computer Science. 2005;3733:284–293.
34. Blondel VD, Guillaume JL, Lambiotte R, Lefebvre E. Fast unfolding of communities in large networks. Journal of Statistical Mechanics: Theory and Experiment. 2008;2008(10):P10008.
35. ; 2009. [Online; accessed 4-March-2014]. Community Detection for NetworkX's Documentation. Available: http://perso.crans.org/aynaud/communities/.

36. Hizanidis J, Kanas V, Bezerianos A, Bountis T. Chimera states in nonlocally coupled networks of Hindmarsh-Rose neuron models. Int J Bif Chaos. 2014;24(3):1450030.
37. Hizanidis J, Kouvaris N, Zamora-Lopéz G, Díaz-Guilera A, Antonopoulos CG. Chimera-like dynamics in modular neural networks. Scientific Reports. 2016;6:19845.
38. Srinivasan R, Russell DP, Edelman GM, Tononi G. Increased synchronization of neuromagnetic responses during conscious perception. The Journal of Neuroscience. 1999;19(13):5435–5448.